Synthesis and NMR Characterization. CPP derivatives are highly curved nanohoops in which the high strain of the macrocycle prevents the direct macrocyclization from linear paraphenylenes.[1] Consequently, Justi and coworkers[1d] reported a synthetic strategy which consists of a Suzuki-Miyaura cross-coupling/macrocyclization between rigidly-curved elements incorporating cyclohexa-2,5-diene moieties as masked benzene rings.[1] The precursor macrocycle thus obtained, is successively aromatized to CPP by reduction in the presence of sodium napthalenide.[1a] On this basis, we have designed the synthesis of **2** by adapting the gram-scale protocol of Jasti and coworkers.[1d] In details, we have selected derivative **6** (Scheme 1), bearing the 9,10-dimethoxy-9,10-dihydroanthracene curved-moiety as a masked anthracene unit, to be coupled by Suzuki-Miyaura reaction with derivative **7**.[1d] The synthesis of **6** is outlined in Scheme 1. Anthraquinone **3** was reacted with (4-bromophenyl)lithium yielding the *syn*-diol **4**, in accordance with the electrostatic model proposed by Justi and coworkers.[1c] Successive deprotonation of **4** with sodium hydride in the presence of MeI afforded derivative **5**, which was converted in diboronate **6** by treatment with isopropyl pinacol borate. Derivative **6** underwent cyclization with **7** in the presence of $Pd(OAc)_2$, S-Phos, and K_3PO_4 in DMF/H_2O, to give macrocycle **8**. This was confirmed by a HR MALDI-FT-ICR mass spectrum, which showed a molecular ion peak at *m*/*z* 894.3895 (Calcd. for $C_{62}H_{54}O_6$, 894.3921). The ^1H NMR spectrum of **8** in $CDCl_3$ (600 MHz, 298 K) showed three OMe singlets at 3.46, 3.41, and 3.15 ppm, in a 1:1:1 ratio, which correlated in the HSQC spectrum (SI) with carbon signals at 52.0 and 52.2 ppm.

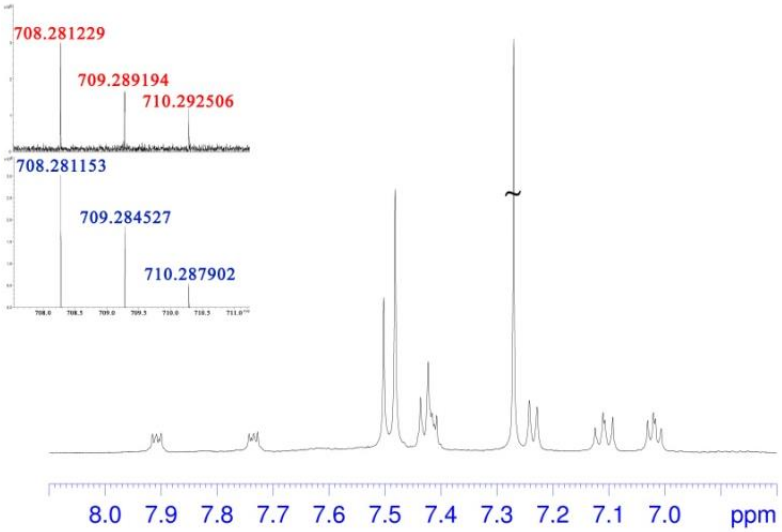

Figure 2. Significant portion of the ^{1}H NMR spectrum of **2** (600 MHz, $CDCl_3$, 298 K). Inset: Significant portion of the isotope pattern in HR MALDI FT ICR mass spectrum of **2**, calculated (in blu) and experimental (in red).

Regarding the cyclohexadienyl moieties of **8**, an AB system was present at 6.03 and 6.11 ppm (J = 10.3 Hz, 4H each), which correlated in the HSQC spectrum (SI) with two resonances at 133.0 and 133.5 ppm. In addition, the aromatic region of the ^{1}H NMR spectrum of **8** evidenced the presence of two AB systems at 7.44/7.38 ppm (J = 8.5 Hz, 4H each) and 7.17/6.92 ppm (J = 8.5 Hz, 4H each) attributable to benzene rings A and B in Scheme 1. Finally, a singlet was present at 7.50 ppm attributable to ArH of ring C (4H). The ^{13}C NMR spectrum of **8** evidenced the diagnostic presence of three singlets (DEPT-135) at 80.3, 74.6, and 74.3 ppm, attributable to the oxygenated carbon atoms.

The treatment of **8** with sodium naphthalenide at −78 °C for 3 h in the dark, in degassed dry THF, followed by quenching with I_2, afforded [8]CPP **2** in 11 % yield. The HR MALDI-FT-ICR mass spectrum of **2** (inset of Figure 2) showed a molecular ion peak at m/z 708.2812 (Calcd. for $C_{56}H_{36}$, 708.2811). A close inspection of the ^{1}H NMR (Figure 2) and DQF-COSY spectra of **2** (SI) in $CDCl_3$ (600 MHz, 298 K) revealed two distinct AA'BB' spin systems attributable to the aromatic hydrogen

atoms 1/2 and 1'/2' (Scheme 1) of the anthracenyl group. In details, the two AA'BB' systems were detected at 7.89/7.39 and 7.72/7.41 ppm (DQF-COSY), and correlated in the HSQC spectrum with four distinct carbon resonances at 127.72, 128.64, 127.64, and 127.12 ppm, respectively.

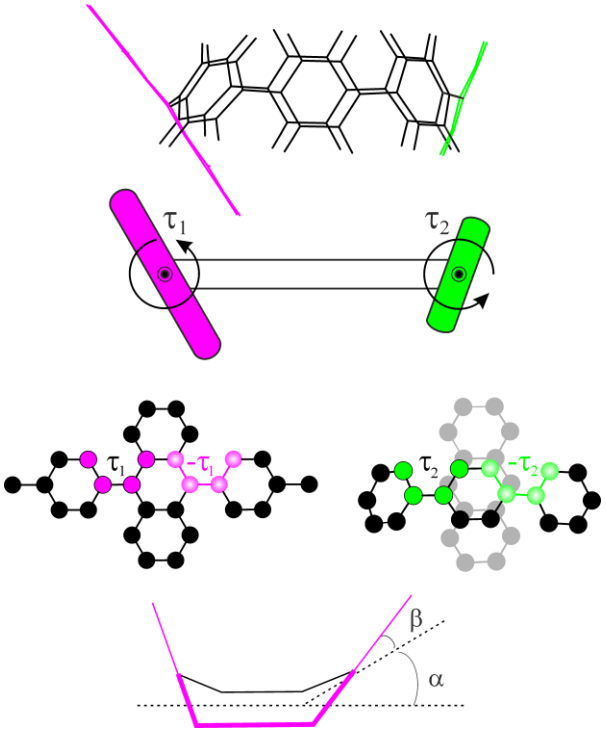

Figure 3. Schematic representation of **2** indicating the dihedral angles τ_1 and τ_2 and the deformation and bent angles α and β.

This result clearly indicates that the two peripheral benzene rings of the anthracenyl group in **2** are nonequivalent because of the their different *in/out* orientation with respect to the CPP cavity, which implies a hindered rotation around τ_1 (Figure 3). Because of this restricted rotation, the benzene ring A, adjacent to the anthracenyl group, adopts an inclined orientation, and the two 3/3' (and 4/4') protons (Scheme 1) become nonequivalent. Consequently, in the ^{1}H NMR spectrum of **2** (SI) two AB systems were detected for the *ortho*-coupled 3/4 and 3'/4' (Scheme 1) protons at 7.11/7.01 (J = 6.1 Hz, 4H) and 7.00/7.08 ppm (J = 9.0 Hz, 4H). VT ^{1}H NMR experiments (400 MHz, $C_2D_2Cl_4$) evidenced no hint of

coalescence up to 493 K for the 1/1', 2/2', 3/3', and 4/4' protons. In addition, the ^{1}H NMR and DQF-COSY spectra of **2** evidenced the presence of an AB system at 7.42/7.23 ppm (J = 8.4 Hz, 8H) attributable to 5/6 H-atoms of ring B (Scheme 1). In fact, because of the fast (with respect to the NMR time scale) rotation around the C-C bond connecting A and B rings, the protons 5 and 5' (and 6/6') become equivalent. Finally, the ArH of rings C and D resonate as two sharp singlets at 7.47 and 7.49 ppm in 2:1 ratio (Figure 2).

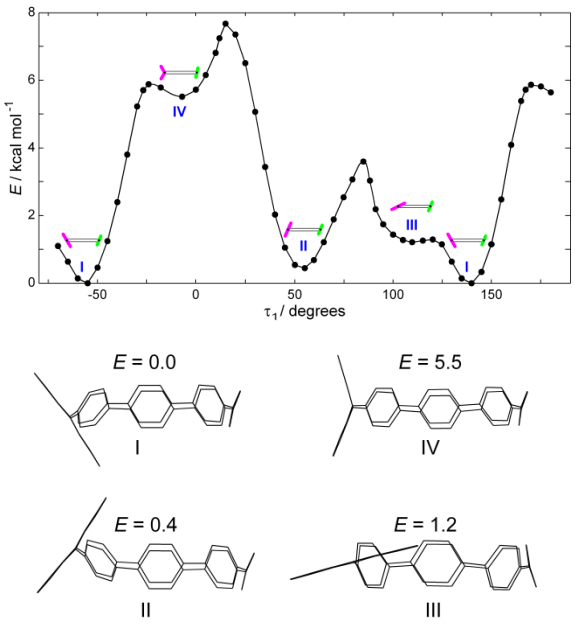

Figure 4. (Top) Potential energy profile (PCM/B97D/TZVP) of **2** along the τ_1 coordinate. Energy is referred to the most stable conformer **I.** (bottom) The most stable conformers of **2** and their relative energies (E / kcal mol^{-1}).

Structural and optoelectronic properties. Since the NMR spectra of **2** suggest the occurrence of a plane of symmetry, geometry optimizations of **2** were initially restricted to the C_s point group. To that end, we computed the optimized potential energy profile along the Lagrangian variable τ_1 (Figure 3), by

fixing in each step the two dependent dihedral angles and performing a full optimization of all the other nuclear coordinates.

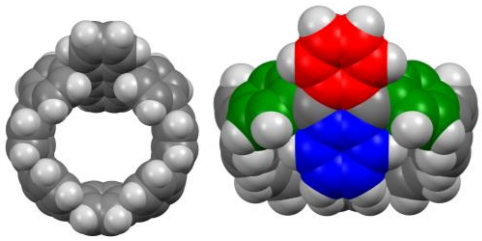

Figure 5. Different views of the optimized structure (DFT calculations, PCM/B97D/TZVP) of **2** (I in Figures 4).

The resulting potential energy profile is reported in Figure 4 (top); four minimum energy structures (I-IV in Figure 4, bottom) have been found, the most relevant of which fall within an energy range of ca 1 kcal/mol. The statistically relevant conformers at room temperature are all characterized by an alternating zig-zag conformation of the phenylene rings, the dihedral angle between neighboring phenylene units being ca 28 degrees, close to the optimal value of 30° found for [*n*]CPP systems.[1,16]

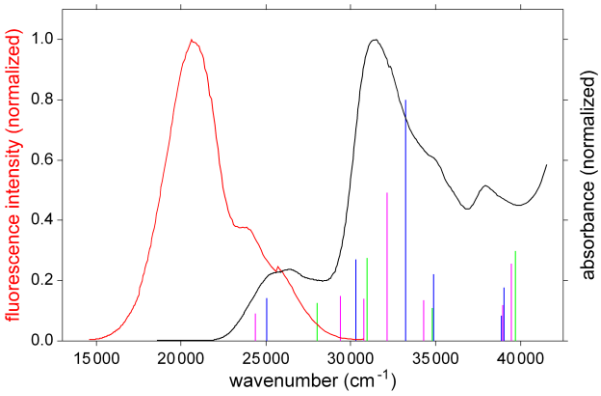

Figure 6. Normalized UV/vis absorption (black) and emission (red) spectra of **2** in CH_2Cl_2 and computed (PCM/TDCAM-B3LYP/6-31+G**) vertical electronic transitions (vertical lines) of conformers I (blue), II (violet), and III (green).

The dihedral angle τ_1 is roughly 60° in both conformers I and II, reaching the expected value for free 9,10 DPA (≈ 77°) only in III. Different stereochemical views of the optimized structure (PCM/B97D/TZVP) of the most stable conformer of **2** are shown in Figure 5. Deformation and bent angles (α and β in Figure 3) amount to 6.2° and 14.2°, respectively, close to the values of 9.3° and 13.7° observed for α and β in the phenyl rings of [8]CPP. These indicate that the steric hindrances between the two peripheral benzene rings (1 and 1′ positions in Scheme 1) of the 9,10-DPA core and the adjacent phenyl rings causes a substantial distortion of the central unit of the anthracene ring, as already found in 1,4-anthracene incorporated [12]CPP's.[5] To ascertain that all the relevant conformations have been actually located, we have also carried out: *i)* geometry optimizations by scanning the τ_2 variable of Figure 3 (SI), and *ii*) geometry optimizations starting from random conformations generated either preserving or relaxing the C_s symmetry. No additional minimum energy conformations were found. Cyclic voltammetry measurements showed that the first oxidation peak of **2** is quasi-reversible (SI), with a half wave potential falling at 0.53 V *vs* Fc^+/Fc redox couple, similar to that found for [8]CPP (0.59 V),[1] but significantly different from that of 1,4-anthracene-incorporated [12]CPP (0.65 V).[5] The first oxidation potential of the most stable conformer (I, SI) is predicted to be at +0.52 V vs Fc^+/Fc by (RO)CAM-B3LYP computations, in excellent agreement with the experimental value. Mulliken spin density analysis shows that the hole in the radical cation $\mathbf{2}^{\cdot+}$ is mainly, but not fully (80%), localized on the anthracene moiety, in line with previous results reported for the 1,4-anthracene-incorporated [12]CPP derivative (1,4-DPA-[12]CPP).[5] Indeed, DFT calculations at PCM-CAM-B3LYP/6-31+G** level predict that the HOMO and LUMO of **2** are mainly localized on the anthracene moiety (Figure 6). The predicted HOMO/LUMO energy gap of **2** is 2.2 eV, significantly lower than that calculated for 1,4-DPA-[12]CPP derivative (3.06 eV).[5] The absorption and the emission spectra of **2** are reported in Figure 6. The absorption spectrum is characterized by an intense band peaked at 320 nm ($\varepsilon = 1.7 \times 10^4$ M^{-1} cm^{-1}) and by a less intense absorption extending from 360 to 450 nm. The former signal is characteristic of [*n*]CPP systems, while the latter resembles very closely that of 9,10-DPA, even though it lacks of its peculiar vibronic structure.

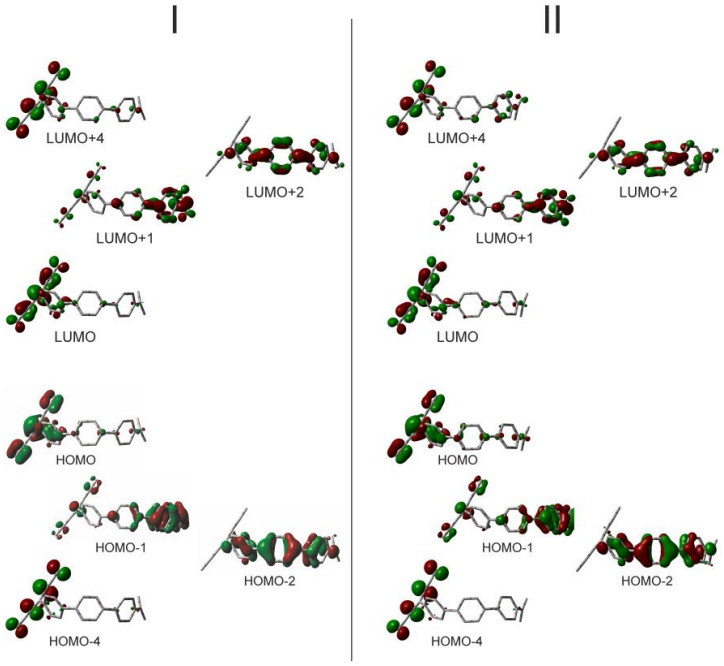

Figure 7. Isodensity surface plots of the frontier Kohn-Sham orbitals of the most populated conformers of **2.**

On the whole, the absorption spectrum of **2** is mainly given by the superposition of the signals of isolated 9,10-DPA and [8]CPP, suggesting that the two molecular moieties maintain in the ground state their own electronic structure, at least as concerns frontier orbitals. The above hypothesis has been checked by theoretical calculations carried out at PCM/TDCAM-B3LYP/6-31+G** level of theory. Predicted lowest energy transitions are reported in Table S1 and sketched in Figure 6, where the computed transition strengths, averaged over Boltzmann conformer populations, are reported as a function of the absorption wavelength and are superimposed to the experimental UV/vis spectrum. Computed optical transitions agree well with the observed absorption spectrum. The broad spectral absorption observed in the region 350-450 nm corresponds to the absorptions predicted at 400, 410, and 380 nm for conformers I, II, and III, respectively (Table S1). The lower symmetry of **2** with respect to

unsubstituted [8]CPP, reflects in a reduced σ-π orbital mixing which makes the HOMO-LUMO absorption, symmetry forbidden in [8]CPP, a bright transition ($f \approx 0.3$, see Table S1).[17] The $S_1 \leftarrow S_0$ transitions predicted at ca 400 nm (Table S1) result from the excitation of one electron from the HOMO to the LUMO, which are both Kohn-Sham π orbitals localized over the 9,10-DPA moiety, as shown in Figure 7. The electronic transitions, which are predicted to fall between 290 and 340 nm, are reported in Table S1 for the three low energy conformers; the involved Kohn-Sham orbitals are sketched in Figure 7 for the two most populated conformers. For conformer I, there are two transitions with significantly higher electric dipole transition moments, falling at 330 and 301 nm. The former transition mainly consists of HOMO-1 → LUMO+1 electron excitation, both levels being mainly localized on the five phenyl rings of CPP which do not belong to DPA, so that electron density changes upon excitation does not significantly involve the DPA moiety, see Figure 7. The transition at 301 nm mainly consists of HOMO-2 → LUMO+1 and HOMO-1 → LUMO+2 electron excitations. The HOMO-2 and LUMO+2 are mainly localized on the six phenylene rings surrounding the DPA moiety and the opposite phenyl ring, thus also this transition does not involve the DPA moiety. The same holds true also for conformers II and III.[18,19,1e,20]

The fluorescence spectrum of **2** is broad, extending from 350 up to 650 nm, with a peak at 485 nm. The slightly structured signal occurring at shorter wavelengths, see Figure 6, is somewhat characteristic of the 9,10-DPA unit, whose emission spectrum in cyclohexane is characterized by vibronic peaks in the region 400-450 nm.[21] By contrast, the emission peak is significantly blue-shifted with respect to that of [8]CPP, whose emission spectrum is peaked at ca. 530 nm,[1e] being more similar to those of [n]CPP hoops, with n>9. It is known that [*n*]CPPs exhibit a large increase in fluorescence quantum efficiencies (Φ) for increasing value of *n*, for [16]CPP Φ=0.9 while for [8]CPP Φ=0.1. The fluorescence quantum yield of **2** has been measured by using the relative method reported by Miller and co-workers.[22] Using quinine sulphate as standard, the fluorescence quantum yield of **2** is Φ = 0.47, which is significantly higher than that observed for [8]CPP and closer to the values observed for larger [9-12]CPP derivatives.[1e] Summarizing, both the emission spectrum and the result of quantum yield measurements

reveal that the emission properties of **2** are more similar to that of nanohoops of higher dimensions. According to TDDFT computations, the electronic excitations of **2** involve Kohn-Sham orbitals which are mainly localized either on the 9,10-DPA moiety or on the remaining five CPP rings (Figure 7). The formation of an excitonic state localized on five phenylene rings, which characterizes the excited state geometries of [n]CPPs with n>8,[16] can also likely occur in **2**, making its emission properties more similar to those of higher size nanohoops.

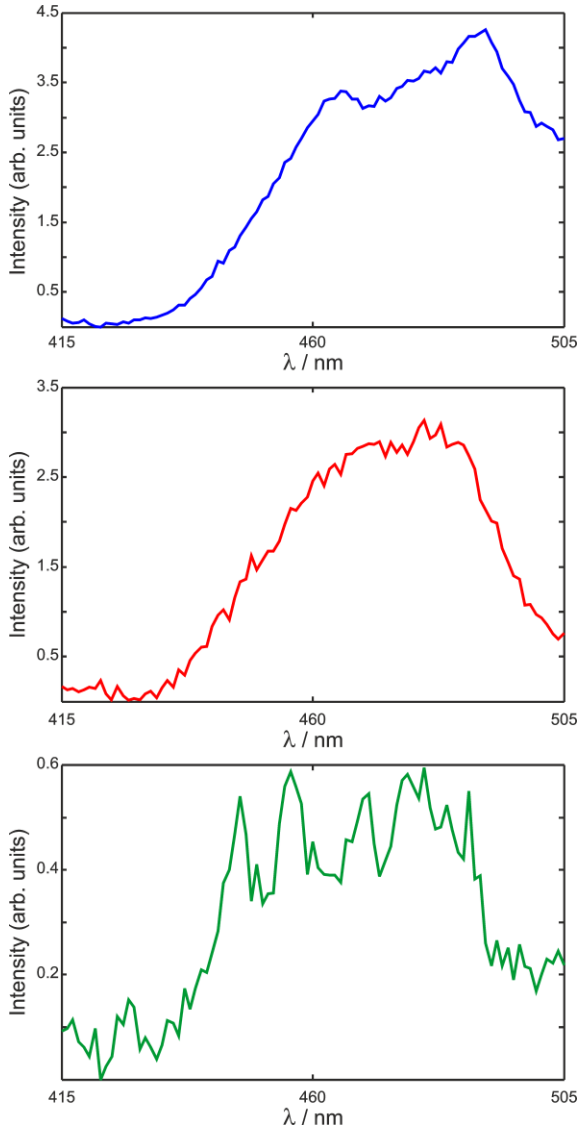

Figure 8. Upconverted emission spectra of **2** (1 mM) and PdOEP in CH_2Cl_2, λ_{exc} = 540 nm. Blue: **[**PdOEP]= 10 μM; red: [PdOEP]= 100 μM; green: [PdOEP]= 1.0 mM. Light source was passed through a 295 nm long pass cut-off emission filter prior to incidence on samples.

9,10-DPA (Figure 1) has been already successfully used as emitter in upconversion of non-coherent light of low intensity, in the presence of a phosphorescent molecule, usually Pd or Pt complexes.[8a] The peculiar properties of **2**, which retains most of spectral features of 9,10-DPA, could indeed make it a potential emitter in low intensity upconversion process. We have thus investigated the optical response of **2** in DCM solution, employing as sensitizer palladium(II) octaethylporphyrin (PdOEP). A few solutions of **2** and PdOEP at different concentration ratios were prepared in anhydrous CH_2Cl_2 under nitrogen atmosphere and then transferred into a quartz cuvette and sealed. Excitation of PdOEP at 540 nm produced the anti-Stokes emissions shown in Figure 8. The shape of the upconverted emission depends on the concentration of the sensitizer, because of the partial overlap with the absorption spectrum of PdOEP. Indeed, at low [PDOEP]/[CPP] concentration ratios the emission profile is much more similar to the normal excitation spectrum, cfr. Figure 6. The slight shoulder appearing at 460 nm is reasonably due to partial reabsorption by the sensitizer in the region 470-520 nm, see Figure S20 of S.I., as also confirmed by the fact that at higher concentration ratios the peak at longer wavelength disappears and the emission band appears flat in the region 460-490 nm, see figure 8. The emission spectrum obtained by up-conversion is significantly red shifted with respect to that previously reported for 9,10-DPA,[8a] demonstrating that emission involves the first excited state of the whole nano-hoop.

Reasonably, the anti-Stokes emission at λ_{exc}= 540 nm takes place via sensitized TTA process. As first pointed out by Parker and Hatchard and deeper investigated by Castellano and coworkers,[23] light upconversion occurring via TTA is characterized, at least at low power density of the incident light, by a quadratic dependence of the emission intensity upon the power of the incident light. To have a better mechanistic insight of the observed anti-Stokes fluorescence, we have investigated the dependence of the emission signal upon excitation light power in the region of low power density. The results are presented in Figure 9, where the upconverted emissions of a solution of **2 (**0.5 mM) and PdOEP (10 μM) in anhydrous CH_2Cl_2 prepared under nitrogen atmosphere and irradiated at different incident power densities (maximum power density ≈ 0.8mW/cm2) are shown.

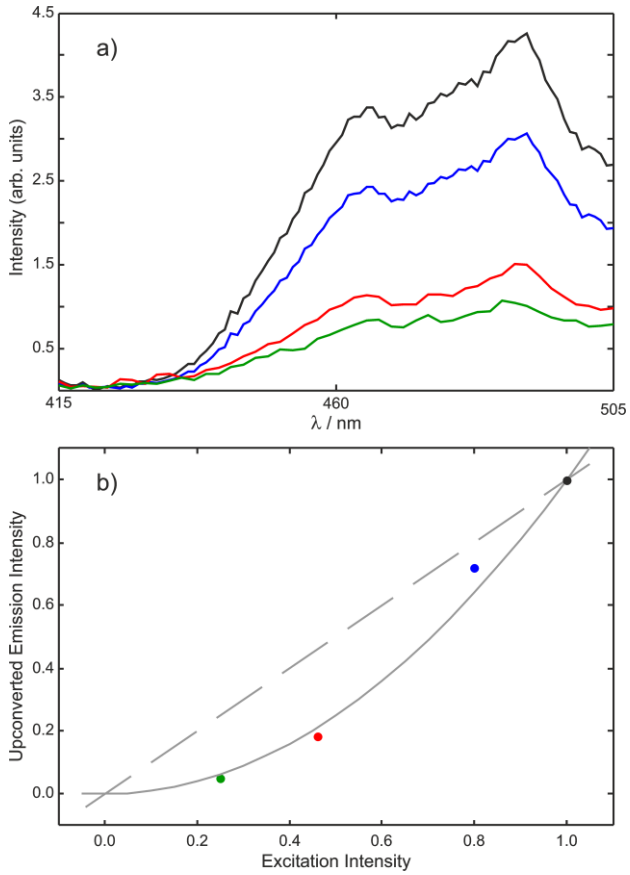

Figure 9. Upconverted emission intensity profiles of a solution of **2** (0.5mM) and PdOEP (10 μM) in dichloromethane at different incident power density (top) and the corresponding normalized integrated emission as a function of the normalized incident power bottom. Dashed line y=x, full line $y=x^2$; maximum incident power 0.8 $mWcm^{-2}$.

The emission band shape is independent of the excitation power. In Figure 9b, the integrated emission intensities of Figure 9a is reported as a function of the power density of the incident light, both normalized at their highest values. Figure 9b clearly indicates that the emission intensity depends on the

square of the power of the incident light, in agreement with previous studies,[23b,c] thus confirming that the upconversion occurs via sensitized TTA.

Conclusions

9,10 anthracene-incorporated [8]cycloparaphenylene has been synthesized adapting the gram-scale synthesis recently reported by Jasti. The compound has been characterized by HR MALDI mass spectroscopy and 1D and 2D NMR spectroscopy, evidencing a Cs symmetry. The absorption spectrum is characterized by two low energy transitions, one at longer wavelength, attributable to the 9,10-DPA, the other falling at wavelengths characteristic of [n]CPP systems. The emission spectrum is however significantly different from [8]CPP one, better resembling that of larger size nano-hoops, both for the peak wavelength and quantum yield. In the presence of the octaethylporphyrin Pd(II) complex as sensitizer, 9,10-anthracene-incorporated [8]CPP undergoes visible light upconversion, the first case reported in the literature in which a cycloparaphenylene derivative is involved as emitter in low power light frequency conversion.

Experimental Section

General Information. HR MALDI mass spectra were recorded on a FT-ICR mass spectrometer equipped with a 7T magnet. The samples were ionized in positive ion mode using ESI positive mode and MALDI ion source. The mass spectra were calibrated externally, and a linear calibration was applied. The samples recorded in MALDI were prepared by mixing 10 μL of analyte in dichloromethane (1 mg/mL) with 10 μL of solution of dithranol (10 mg/mL in THF). Tetrahydrofuran was dried by heating under reflux over sodium wire in the presence of benzophenone as indicator while dimethylformamide were dried by activated 3 Å molecular sieves. All chemicals reagents grade were used without further purification and were used as purchased. Derivative **7**[1d] and sodium naphthalenide[1a] were prepared in accord to reported procedures.[1d] Reaction temperatures were measured externally. Reactions were monitored by TLC silica gel plates (0.25 mm) and visualized by UV light

254 nm, or by spraying with H_2SO_4−$Ce(SO_4)_2$. NMR spectra were recorded on a 600 [600 (^{1}H) and 150 MHz (^{13}C)], 400 [400 (^{1}H) and 100 MHz (^{13}C)], 300 MHz [300 (^{1}H) and 75 MHz (^{13}C)] or 250 MHz [250 (^{1}H) and 62.5 MHz (^{13}C)] spectrometer. Chemical shifts are reported relative to the residual solvent peak.

Computational details. Constrained and unconstrained geometry optimizations were carried at the density functional level of theory (DFT), by using the B97D functional including the empirical correction for dispersion energy proposed by Grimme,[24] in conjunction with the density fitting approximation and the TZVP basis set. The nature of the stationary points was verified by computing the eigenvalues of the Hessian matrix. B97D was chosen because it has been proven to be the most accurate method in predicting torsional barriers of substituted biphenyls.[25] Time dependent (TD) DFT computations were carried out by using the CAM-B3LYP range-separated hybrid functional.[26] Indeed, it is well known that electronic excitations in conjugated oligomers have a charge transfer nature, with structural distortions that can be modelled only with the use of range-corrected hybrid DFT models including long range electronic exchange interactions[16,27] The same functional was adopted for the computation of the first oxidation potential. The restricted open shell (RO) formalism was used because it yields more accurate oxidation potentials when used with the CAM-B3LYP functional. The absolute potential of Fc^+/Fc in dichloromethane has been set to 4.98 V.[28] The 6-31+G(d,p) basis set was adopted for all the computations employing the CAM-B3LYP functional. Effects due to solvent (dichloromethane) polarization were included in all computations by the polarizable continuum model (PCM).[29] DFT and TDDFT computations were carried out by using the Gaussian program.[30]

Optoelectronic characterization. Optical absorption spectra were measured on a Cary 50 UV-vis spectrophotometer from Varian. Steady-state luminescence spectra were recorded on a modular fluorescence spectrometer from Acton Research, equipped with a xenon lamp. Light source was passed through a 295 nm long pass cut-off emission filter prior to incidence on the sample. All solution samples were deaerated with nitrogen. Relative quantum yields of **2** in dichloromethane were determined as described by Williams using quinine sulfate (0.1 M H2SO4) as standard. Excitation

occurred at 319 nm and the fluorescence of **2** was integrated from 350 – 650 nm, both for 2 and for quinine sulphate. In up-conversion measurements an additional longpass filter cutting at ca. 300 nm has been employed to completely cut down possible emission produced by excitation of second order diffraction. The quantum yield measurements were performed in accord with the method reported by Miller and co-workers.[23] The CPP **2** solutions were diluted to give absorbance values in the range 0.02-0.35, within the expected linear calibration range of fluorescence emission versus concentration. The quantum yields were calculated according to equation reported by Miller.

$$\Phi_X = \Phi_R \frac{I_X}{I_R} \frac{A_R}{A_X} \frac{\eta_X^2}{\eta_R^2}$$

Φ_R is the quantum yield of the standard, A is the absorbance of the solution, I is the integrated intensity of the exciting light and η is the average refractive index of the solution. Subscripts R and X refer to the reference and unknown compound, respectively. Cyclic voltammetry measurements were performed in CH_2Cl_2 with TBAP as electrolyte. All potentials were referenced to the platinum quasi-reference electrode. The potential has been calibrated with ferrocene/ferrocenium (Fc/Fc^+) redox couple.

Derivative 5. 1,4-Dibromobenzene (10.0 g, 42.4 mmol) was dissolved in 450 mL of dry THF and cooled to –78 °C. To this solution was added a 2.5 M solution of *n*-butyllithium in *n*-hexane (18.2 mL, 45.5 mmol) over 15 min and the reaction mixture was stirred for 30 min. Anthraquinone (4.31 g, 20.7 mmol) was added to the reaction mixture in three equal portions over 30 min. The solution was stirred for 2 h at –78 °C and then added to 180 mL of water. The mixture was further diluted by the addition of 180 mL of diethyl ether and the organic layer was separated. The aqueous layer was extracted with diethyl ether (3 x 70 mL) and the combined organic layers were washed with a saturated brine solution (100 mL). The organic phase was then dried over sodium sulfate, filtered and evaporated under reduced pressure to give the diol product **4** which was used without further purification. The diol **4** was dissolved in 70 mL of dry THF and sodium hydride (2.07 g, 51.7 mmol, 60% in mineral oil) was added at 0 °C. The mixture was stirred for 30 min and methyl iodide (5.2 mL, 83 mmol) was added. The mixture was

allowed to warm to room temperature and stirred for an additional 18 h. The excess of sodium hydride was then quenched by addition of 100 mL of water and filtered. The white solid was washed with 120 mL of ethyl ether and dried in vacuum for 12 h, to give **5** in 53% of yield (6.04 g). M. p. > 310 °C dec. ^{1}H NMR (400 MHz, 298 K, $CDCl_3$): δ (ppm) 7.49 (m, 4H, Ar-H), 7.30 - 7.33 (overlapped, 8H, Ar-H), 7.19 (d, J = 8.5 Hz, 4H, Ar-H), 2.93 (s, 6H, OMe); ^{13}C NMR (100 MHz, $CDCl_3$): δ (ppm) 147.9, 138.2, 131.0, 128.7, 128.2, 121.1, 78.7, 51.3. HRMS (ESI+): m/z $[M+Na]^+$ calculated for $C_{28}H_{22}Br_2NaO_2$: 572.9864, found 572.9859.

Derivative 6. 5 (2.53 g, 4.77 mmol) was dissolved in 280 mL of dry THF and cooled to –78 °C. Then a 2.5 M solution of *n*-butyllithium in hexane (9 mL, 22.5 mmol) was added over 10 min. Then isopropyl pinacol borate (8.50 mL, 42.0 mmol) was added rapidly and the solution was stirred for 5 h under argon. 200 mL of water and 100 mL of ethyl acetate were added to the solution and the biphasic mixture was stirred for 30 min at room temperature. The organic phase was extracted and the aqueous layer was washed with ethyl acetate (3 x 70 mL). The combined organic layers were dried over sodium sulfate, filtered and concentrated in vacuum to give a colorless oil that was purified by chromatography on silica gel (hexane/ethyl acetate, 7:3). The product **6** was obtained as a white solid in 41% of yield (1.30 g). M.p.: 252.2-253.3°C. ^{1}H NMR (400 MHz, 298 K, $CDCl_3$): δ (ppm) 7.68 (d, J = 8.1 Hz, 4H, Ar-H), 7.48 (m, 4H, Ar-H), 7.43 (d, J = 8.1 Hz, 4H, Ar-H), 7.24 (m, 4H, Ar-H), 2.94 (s, 6H, OMe), 1.30 (s, 24H, CH_3); ^{13}C NMR (62.5 MHz, $CDCl_3$): δ (ppm) 152.1, 138.5, 134.5, 128.5, 128.4, 126.2, 83.8, 79.0, 51.2, 25.0. HRMS (ESI+): m/z $[M+Na]^+$ calculated for $C_{40}H_{46}B_2NaO_6$: 667.3378, found 667.3380.

Derivative 8. Dibromide **7** (1.99 g, 3.00 mmol), diboronate **6** (1.93 g, 3.00 mmol), S-Phos (246 mg, 0.61 mmol) and K_3PO_4 (2.55 g, 12.0 mmol) in a mixture of DMF/H_2O (600 mL/60mL) was mixed and degassed twice through freeze/pump/thaw technique. Then $Pd(OAc)_2$ (471 mg, 2.11 mmol) was added and the mixture was stirred at 100 °C for 19 h under argon. After cooling to room temperature, the mixture was filtered through a short plug of Celite® and added to 150 mL of water and 100 mL of $CHCl_3$. The biphasic mixture was stirred for 30 min and separated. The aqueous layer was washed with $CHCl_3$ (3 x 80 mL). The combined organic layers were washed with 200 mL of a saturated brine solution and dried over sodium sulfate. After filtration the solvent was evaporated under vacuum, the

crude mixture was purified by column chromatography on silica gel (Hexane/CH_2Cl_2/Et_2O = 29:70:1) to give the macrocycle **8** as a white solid in 10 % of yield (0.27 g). M. p. > 305 °C dec. ^{1}H NMR (600 MHz, 298 K, $CDCl_3$): δ (ppm) 7.85 (m, 4H, Ar-H), 7.50 (s, 4H, Ar), 7.47 (m, 4H, Ar-H), 7.44 (d, J = 8.5 Hz, 4H, CH=CH), 7.38 (d, J = 8.5 Hz, 4H, CH=CH), 7.17 (d, J = 8.5 Hz, 4H, CH=CH), 6.92 (d, J = 8.5 Hz, 4H, CH=CH), 6.11 (d, J = 10.3 Hz, 4H, CH=CH), 6.03 (d, J = 10.3 Hz, 4H, CH=CH), 3.46 (s, 6H, OMe), 3.41 (s, 6H, OMe), 3.15 (s, 6H, OMe). ^{13}C NMR (150 MHz, 298 K, $CDCl_3$): δ (ppm) 145.0, 143.4, 142.8, 139.8, 139.5, 138.6, 133.5, 133.0, 128.3, 127.5, 126.9, 126.3, 126.1, 80.3, 74.6, 74.3, 52.2, 52.0. DEPT-135 (150 MHz, $CDCl_3$): δ (ppm) 133.5, 133.0, 128.3, 127.5, 126.9, 126.3, 126.1, 52.2, 52.0. HRMS (MALDI): m/z M+ calculated for $C_{62}H_{54}O_6$: 894.3921, found 894.3895.

Derivative 2. Derivative **8** (225 mg, 0.25 mmol) was dissolved in 18 mL of dry THF, under argon, and the solution was degassed through freeze/pump/thaw technique and cooled to –78 ℃. Then, a solution of sodium naphthalenide in dry THF, freshly prepared (2.7 mL, 2.7 mmol) was added and the reaction mixture was stirred for 3 h at –78 ℃. Then I_2 was added (3 mL of a 1.0 M solution in THF) and the reaction mixture was warmed at room temperature. Subsequently a saturated solution of sodium thiosulfate (50 mL) and $CHCl_3$ (50 mL) were added, and the reaction mixture was stirred for 10 min. The organic layer was extracted and the aqueous phase was washed with $CHCl_3$ (3 x 50 mL) and finally the combined organic layers was washed with a saturated brine solution (60 mL) and dried over sodium sulfate and filtered. The solvent was removed under reduced pressure, and the crude product was purified by chromatography column on silica gel under nitrogen flow (*n*-hexane/CH_2Cl_2 = 3:7), to give the product **2** as a yellow solid in 11 % of yield (19 mg). M. p. > 285 °C dec. ^{1}H NMR (600 MHz, 298 K, $CDCl_3$): δ (ppm) 7.89 (m, 2H, Ar-H), 7.72 (m, 2H, Ar-H), 7.49 (s, 4H, Ar-H), 7.47 (s, 8H, Ar-H), 7.42-7.40 (overlapped, 8H, Ar-H), 7.22 (d, J = 8.3 Hz, 4H, Ar-H), 7.11-7.08 (overlapped, 4H, Ar-H), 7.02-7.00 (overlapped, 4H, Ar-H). ^{13}C NMR (150 MHz, $CDCl_3$): δ (ppm) 146.6, 146.5, 142.7, 140.3, 139.7, 138.8, 138.4, 137.2, 137.0, 136.9, 128.6, 128.3, 128.0, 127.9, 127.8, 127.7, 127.6, 127.5, 127.5, 127.4, 127.2, 127.1, 127.1. DEPT-135 (150 MHz, $CDCl_3$): δ (ppm) 128.6, 128.3, 128.0, 127.9, 127.8,

127.7, 127.6, 127.5, 127.5, 127.4, 127.2, 127.10, 127.12. HRMS (MALDI): *m/z* M^+ calculated for $C_{56}H_{36}$: 708.2811, found 708.2812.

Acknowledgements

The authors acknowledge the Regione Campania (POR CAMPANIA FESR 2007/2013 O.O.2.1, B46D14002660009, "Il potenziamento e la riqualificazione del sistema delle infrastrutture nel settore dell'istruzione, della formazione e della ricerca"), for the FT-ICR mass spectrometer facilities, the Centro di Tecnologie Integrate per la Salute (CITIS, Project PONa3_00138), Università di Salerno, for the 600 MHz NMR facilities.

Supporting Information: Copies of 1D, 2D NMR and HR MS spectra of new compounds, UV−vis absorption and fluorescence spectra of **2**, cyclic voltammetry of **2**, emission spectrum of **2** in dichloromethane at λ_{exc} = 390 nm, emission spectrum of **2** in dichloromethane at λ_{exc} = 484 nm, cartesian coordinates of the conformer I and III (Figure 4), this material is available free of charge via the Internet at http://pubs.acs.org.

REFERENCES

[1](a) Jasti, R.; Bhattacharjee, J.; Neaton, J. B.; Bertozzi, C. R. *J. Am. Chem. Soc*. **2008**, *130*, 17646–17647. (b) Segawa, Y.; Miyamoto, S.; Omachi, H.; Matsuura, S.; Senel, P.; Sasamori, T.; Tokitoh, N.; Itami, K. *Angew. Chem., Int. Ed.* **2011**, *50*, 3244–3248. (c) Sisto, T. J.; Golder, M. R.; Hirst, E. S.; Jasti, R. *J. Am. Chem. Soc.* **2011**, *133*, 15800–15802. (d) Xia, J.; Bacon, J. W.; Jasti, R. *Chem. Sci.* **2012**, *3*, 3018–3021. (e) Darzi, E. R.; Jasti, R. *Chem. Soc. Rev.*, **2015**, *44*, 6401–6410. (f) Lewis, S. E. *Chem. Soc. Rev.*, **2015**, *44*, 2221–2304. (g) Zabula, A. V.; Filatov, A. S.; Xia, J.; Jasti, R.; Petrukhina, M. A. *Angew. Chem., Int. Ed.* **2013**, *52*, 5033−5036.

[2](a) Omachi, H.; Nakayama, T.; Takahashi, E. ; Segawa, Y. ; Itami, K. *Nat. Chem.* **2013**, *5*, 572–576. (b) Segawa, Y.; Yagi, A.; Matsui, K.; Itami, K. *Angew. Chem. Int. Ed*, **2016**, *55*, 5136–5158. (c) Golling, F. E.; Quernheim, M.; Wagner, M.; Nishiuchi, T.; Müllen, K. *Angew. Chem. Int. Ed.* **2014,** *53*, 1525−1528. (d) Omachi, H.; Segawa, Y.; Itami, K. *Acc. Chem. Res.* **2012**, *45*, 1378–1389.

[3](a) Iwamoto, T.; Watanabe, Y.; Sadahiro, T.; Haino, T.; Yamago, S. *Angew. Chem., Int. Ed.* **2011**, *50*, 8342–8344. (b) Iwamoto, T.; Slanina, Z.; Mizorogi, N.; Guo, J.; Akasaka, T.; Nagase, S.; Takaya, H.; Yasuda, N.; Kato, T.; Yamago, S. *Chem. Eur. J.* **2014**, *20*, 14403 – 14409. (c) Nakanishi, Y.; Omachi, H.; Matsuura, S.; Miyata, Y.; Kitaura, R.; Segawa, Y.; Itami, K.; Shinohara, H. *Angew. Chem. Int. Ed.* **2014**, *53*, 3102 –3106. (d) Ueno, H.; Nishihara, T.; Segawa, Y.; Itami, K. *Angew. Chem. Int. Ed.* **2015**, *54*, 3707 –3711. (e) Lee, S.; Chénard, E.; Gray, D. L.; Moore, S. J. *J. Am. Chem. Soc.* **2016,** *138*, 13814–13817. (f) Very recently, Yamago and coworkers reported an example of inclusion of [n]CPPs inside [n+5]CPPs macrocycles: Hashimoto, S.; Iwamoto, T.; Kurachi, D.; Kayahara, E.; Yamago, S. *ChemPlusChem* **2017**, *82*, 1015−1020.

[4] Della Sala, P.; Talotta, C.; Caruso, M.; De Rosa, M.; Soriente, A.; Neri, P.; Gaeta, C. *J. Org. Chem.* **2017**, *82*, 9885−9889. C. Talotta, C. Gaeta, M. De Rosa, J. R. Ascenso, P. M. Marcos, P. Neri, *Eur. J. Org. Chem.* **2016**, *1*, 158-167. De Rosa, M.; Talotta, C.; Soriente, A. *Lett. Org. Chem.* **2009**, *6*, 301−305.

[5] Li, P.; Wong, B. M.; Zakharov, L. N.; Jasti, R. *Org. Lett.*, **2016**, *18*, 1574−1577.

[6](a) Yagi, A.; Segawa, Y.; Itami, K. *J. Am. Chem. Soc.*, **2012**, *134*, 2962–2965. (b) Omachi, H.; Segawa, Y.; Itami, K. *Org. Lett.*, **2011**, *13*, 2480–2483. (c) Farajidizaji, B.; Huang, C.; Thakellapalli, H.; Li, S.; Akhmedov, N. G.; Popp, B. V.; Petersen, J. L.; Wang, K. K. *J. Org. Chem.* **2017**, *82*, 4458–4464.

[7](a) Thakellapalli, H.; Farajidizaji, B.; Butcher, T. W.; Akhmedov, N. G.; Popp, B. V.; Petersen, J. L.; Wang, K. K. *Org. Lett.*, **2015**, *17*, 3470–3473. (b) Matsui, K.; Segawa, Y.; Itami, K. *Org. Lett.*, **2012**, *14*, 1888–1891. (c) Hayase, N.; Miyauchi, Y.; Aida, Y.; Sugiyama, H.; Uekusa, H.; Shibata, Y.; Tanaka,

K. *Org. Lett.* **2017**, *19*, 2993-2996. (d) Nishigaki, S.; Fukui, M. Sugiyama, H.; Uekusa, H.; Kawauchi, S.; Shibata, Y.; Tanaka, K. *Chem. Eur. J.* **2017,** *23*, 7227-7231.

[8] (a) Baluschev, S.; Miteva, T.; Yakutkin, V.; Nelles, G.; Yasuda, A.; Wegner, G. *PhysRevLett* **2006**, *97*, 143903-1-143903-3. (b) Singh-Rachford, T. N.; Castellano, F. N. *Coord. Chem. Rev.*, **2010**, *254*, 2560–2573.

[9]Monguzzi, A.; Braga, D.; Gandini, M.; Holmberg, V. C.; Kim, D. K.; Sahu, A.; Norris, D. J.; Meinardi, F. *Nano Lett.* **2014**, *14*, 6644−6650.

[10](a) Khnayzer, R. S.; Blumhoff, J.; Harrington, J. A.; Haefele, A.; Deng, F. ; Castellano, F. N. *Chem. Commun.* **2012**, *48*, 209‐211. (b) Ye, C.; Wang, J.; Wang, X.; Ding, P.; Liang, Z.; Tao, X. *Phys. Chem. Chem. Phys.* **2016**, *18*, 3430‐3437.

[11]Liu, Q.; Feng, W.; Yang, T.; Yi, T.; Li, F. *Nat. Protoc.* **2013**, *8*, 2033‐2044.

[12] (a) Koslov, D. V.; Castellano, F. N. *Chem. Commun.* **2004**, 2860–2861. (b) Islangulov, R. R.; Lott, J.; Weder, C.; Castellano, F. N. *J. Am. Chem. Soc.* **2007**, *129*, 12652–12653. (c) Keivanidis, P. E.; Baluschev, S.; Miteva, T.; Nelles, G.; Scherf, U.; Yasuda, A.; Wegner, G. *Adv. Mater.* **2003**, *15*, 2095–2098.

[13] Baluschev, S.; Yakutkin, V.; Miteva, T.; Wegner, G.; Roberts, T.; Nelles, G.; Yasuda, A.; Chernov, S.; Aleshchenkov, S.; Cheprakov, A. *New J. Phys.* **2008,** *10*, 013007/1.

[14] Liu, Q.; Yang, T.; Feng, W.; Li, F. *J. Am. Chem. Soc*., **2012**, *134*, 5390−5397.

[15] Duan, P.; Yanai, N.; Nagatomi, H.; Kimizuka, N. *J. Am. Chem. Soc*., **2015**, *137*, 1887−1894.

[16]Adamska, L.; Nayyar, I.; Chen, H.; Swan, A. K.; Oldani, N.; Fernandez-Alberti, S.; Golder, M. R.; Jasti, R.; Doorn, S. K.; Tretiak, S. *Nano Lett.* **2014**, *14*, 6539-6546.

[17] Iwamoto, T.; Watanabe, Y.; Sakamoto, Y.; Suzuki, T.; Yamago, S. *J. Am. Chem. Soc*., **2011**,*133*, 8354−8361.

[18]Fujitsuka, M.; Cho, D. W.; Iwamoto, T.; Yamago, S.; Majima, T. *Phys Chem. Chem. Phys*. **2012**, *14*, 14585−14588.

[19]Segawa, Y.; Fukazawa, A.; Matsuura, S.; Omachi, H.; Yamaguchi, S.; Irle, S.; Itami, K. *Org. Biomol. Chem.,* **2012,** *10*, 5979−5984.

[20]Golder, M. R.; Jasti, R. *Acc. Chem. Res.* **2015,** *48*, 557-566.

[21]Du, H.; Fuh, R.-C. A.; Li, J.; Corkan, L. A.; Lindsey, J. S.; *Photochem. Photobiol.* **1998**, *68*, 141-142

[22]Williams, A. T. R.; Winfield, S. A.; Miller, J. N. *Analyst*, **1983**, *108*, 1067-1071.

[23] (a) Parker, C. A.; Hatchard, C. G. *Proc. Chem Soc.,* London **1962**, 386-387. (b) Haefele, A.; Blumhoff, J.; Khnayzer, R. S.; Castellano, F. N. *J. Phys. Chem. Lett.* **2012**, *3*, 299-303. (c) Deng, F.; Blumhoff, J.; Castellano, F. N. *J. Phys. Chem. A* **2013**, *117*, 4412,4419.

[24]Schwabe, T.; Grimme, S. *Phys. Chem. Chem. Phys.* **2006**, *8*, 4398−4401

[25]Masson, E. *Org. Biomol. Chem.* **2013**, *11*, 2859-2871.

[26]Yanai, T.; Tew, D. P.; Handy, N. C. *Chem. Phys. Lett.* **2004**, *393*, 51-57.

[27]Capobianco, A.; Borrelli, R.; Landi, A.; Velardo, A.; Peluso, A. *J Phys. Chem A*, **2016,** *120,* 5581-5589.

[28]Capobianco, A.; Velardo, A.; Peluso, A. *Comp. Theor. Chem*. **2015,** *1070,* 68-75; Capobianco, A.; Caruso, T.; Peluso, A. *Phys. Chem. Chem. Phys*. **2015**, *17*, 4750-4756.

[29]Miertuš, S.; Scrocco, E.; Tomasi, *J. Chem. Phys.* **1981,** *55*, 117-129.

[30][G09]Frisch, M. J.; et al. *Gaussian 09*, Revision D.01; Gaussian Inc.: Wallingford, CT, 2009.